

Surface normal estimation from polarization and shading under the convexity assumption

Daisuke Miyazaki · Naoki Kodama

Received: date / Accepted: date

Abstract Polarization is useful for estimating surface normals. In this paper, polarization is applied to shape estimation. Surface normal estimation from a single image is commonly performed by shape-from-shading. An alternative approach is shape-from-polarization, which usually cannot uniquely determine the surface normal and must be accompanied by additional information. The shading information is a promising option, but if the index of refraction is unknown, the surface normal is still non-uniquely determined. To resolve this problem, we assume that the object surface is locally convex. Under this assumption, we show that the surface normal can be uniquely determined from the gradients of the shading information. Our method works when the light and camera are closely arranged.

Keywords Polarization · Shape-from-X · Surface normal · Shape-from-shading

1 Introduction

Polarization information can be exploited in shape estimation. The polarization state of the light reflected from a surface depends on the surface normal of

D. Miyazaki
Hiroshima City University
3-4-1 Ozukahigashi Asaminami-ku, Hiroshima city, JAPAN
Tel.: +81-82-830-1500
Fax: +81-82-830-1656
E-mail: miyazaki@hiroshima-cu.ac.jp

N. Kodama
Hiroshima City University
3-4-1 Ozukahigashi Asaminami-ku, Hiroshima city, JAPAN
Tel.: +81-82-830-1500
Fax: +81-82-830-1656
E-mail: naoki.kodama@ime.info.hiroshima-cu.ac.jp
Present address: ASTEC Co., Ltd., JAPAN

the object. Therefore, polarization can provide rich shape information about the surface normal, although the surface normals extracted by shape-from-polarization are non-unique.

Alternatively, shape estimation can be obtained from the shading information. Because shading is caused by both the surface normal and the light source, it provides rich shape information about the surface normal. However, as is well-known, photometric stereo requires three images to obtain the surface normal of a target shape. Meanwhile, shape-from-shading, which uses a single image, is insufficient for determining surface normals.

To resolve these problems, this paper proposes a method that estimates a surface normal using both the polarization and shading information.

1.1 Related works

Surface normals from a single image are extracted by two main approaches: shape-from-shading and shape-from-polarization.

Shape-from-shading [1–6] estimates the surface normal of a target object from the object-shading information. Unlike photometric stereo, which uses three or more images illuminated from different directions, shape-from-shading uses a single image illuminated by a single light source. The authors of [7] mathematically proved that the surface normal can be estimated from three images under different light directions, whereas shape-from-shading, which uses a single image, is an ill-posed problem. Some previously proposed methods [3, 5, 6] solved this problem by making additional assumptions. However, some of these assumptions are inapplicable in real-world situations. The applicability of these approaches can be broadened by obtaining additional input data.

Polarization analysis is also useful for estimating the surface normals of objects. Wolff and Boulton [8] proved that polarization analysis from two viewpoints can estimate a surface normal if the corresponding points are known. Rahmann and Canterakis [9] estimated the surface normal of a specular object from multiple viewpoints by iteratively finding the corresponding points of these viewpoints. Rahmann [10] proved that iterating the search for corresponding points obtains only the quadratic surfaces of objects. Atkinson and Hancock [11] found the corresponding points between two viewpoints of the local structure of an object and calculated the surface normal from the polarizations of these two viewpoints. Atkinson and Hancock [12] also estimated the surface normal of a diffuse object from a single viewpoint. Huynh et al. [13] estimated both the surface normal and refractive index of an object.

Polarization is useful not only for photometric stereo [14–18] but also for shape-from-shading [19, 20]. Mahmoud et al. [19] solved the shape-from-shading problem by a polarization-based approach. They used the degree and angle of the polarization during diffuse reflection. However, the shape-from-polarization approach obtains two surface normal candidates, whereas the shading information uniquely determines the correct candidate. Smith et al.

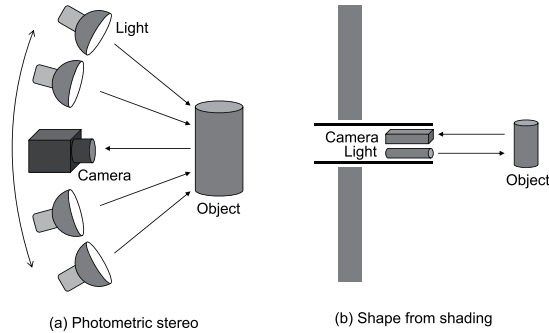


Fig. 1 Photometric stereo and shape-from-shading in (a) an open environment with movable light sources and (b) a limited environment with an immovable single light source

[20] similarly used the degree and angle of polarization during diffuse reflection and added some priors to estimate the surface normal.

Our proposed approach solves the shape-from-polarization problem with shading because polarization cannot uniquely determine the surface normal [8]. Previous polarization-based approaches [19,20] used the degree of polarization, which depends on the index of refraction and surface roughness of the target object. As both parameters are usually unknown, our method obtains two surface normal candidates and determines the correct candidate from the shading information rather than from the polarization degree.

1.2 Our work

Existing shading-based shape-from-polarization methods [19,20] require different directions of the light source and the camera. We set the light source close to the camera because this configuration is widely applicable. In a sufficiently large space, photometric stereo is preferable because the light source can be moved (see Fig. 1 (a)). Conversely, in a confined space with little room for moving the light source, the light must be positioned near the camera (Fig. 1 (b)). In this situation, shape-from-shading is used rather than photometric stereo processing. The proposed method assumes that the light source is close to the camera. This configuration typifies various applications, such as endoscopic measurements.

The characteristics of our method are summarized below:

- The surface normal of the object is obtained from a single image captured by a polarization camera. If the camera and polarizing filter are separated, three images are required, which should be captured from different filter angles by the same camera.
- The light cast on the object is generated from a single point source set far from the object. This light source should be unpolarized. We assume that

the lighting direction almost aligns with the viewing direction, meaning that the light source direction is known.

- The shading information and the polarization information are input to the model. We input the phase angle of the polarization, not the degree of polarization.
- Reflection from the target object is assumed as diffuse and not specular. Because it needs the diffuse reflection, our method is applicable to bright opaque dielectrics, and is inapplicable to metals, transparent objects, and black opaque dielectrics.
- The object is assumed as a single-color object, implying constant reflectance and no textures.
- The surface normal heading towards the light source (and the camera) is assumed to be observed.
- The surface normal is assumed to be differentiable, meaning that the object surface is geometrically smooth.
- The object is assumed to be locally convex. The method can be applied to globally non-convex objects, but is invalid on the locally concave part. By “locally convex,” we mean that the four neighboring pixels (from which we calculate the gradient of the discretized image) are convex.
- We assume no inter-reflections.
- We do not require the index of refraction, and we do not require the surface roughness parameter.

2 Lambert reflection

When an object obeys the Lambertian reflection model and the light source is an infinitely far single light, the observed brightness I can be calculated as

$$I = \rho \mathbf{n} \cdot \mathbf{l}. \quad (1)$$

The unit vector $\mathbf{l} = (l_x, l_y, l_z)^\top$ in Eq. (1), referred to as the light vector, indicates the direction of the light source. Diffuse reflection is modeled by Lambert’s law, which represents the shading as the dot-product of $\mathbf{l} = (l_x, l_y, l_z)^\top$ and another unit vector representing the surface normal $\mathbf{n} = (n_x, n_y, n_z)^\top$. The diffuse reflectance (hereafter called the albedo) is denoted ρ . Note that, Eq. (1) becomes negative if the angle between \mathbf{n} and \mathbf{l} exceeds 90° but the actual brightness cannot be lower than zero.

The proposed method assumes a single-colored target object with no specular reflections. Denoting the angle between \mathbf{n} and \mathbf{l} as θ , Eq. (1) can be rewritten as

$$\mathbf{n} \cdot \mathbf{l} = |\mathbf{n}| \cdot |\mathbf{l}| \cos \theta. \quad (2)$$

The maximum of $\mathbf{n} \cdot \mathbf{l}$ is 1 because the maximum of $\cos \theta$ is 1 and both \mathbf{n} and \mathbf{l} are unit vectors. The maximum brightness I among all pixels equals the albedo ρ because the surface is assumed closed and smooth with a single albedo that obeys Lambert diffuse reflection. Therefore, to determine ρ , we find the maximum brightness I among all pixels in the object region.

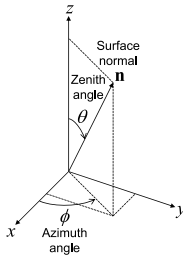


Fig. 2 Polar coordinates of the surface normal

3 Shape extraction from polarization

3.1 Polarization

Circular polarization is not related to the proposed method; therefore, we consider only linear polarization here. When an electromagnetic wave (such as light) oscillates in only one direction, it is perfectly linearly polarized, whereas an electromagnetic wave oscillating isotropically in all directions is completely unpolarized.

As the polarizer is rotated, the light intensity periodically varies between its maximum value I_{\max} and its minimum value I_{\min} . In this paper, the polarizer angle at which I_{\min} is observed is called the azimuth angle ϕ . The surface normal is represented in polar coordinates (ϕ, θ) , where θ is the zenith angle (see Fig. 2). Because a linear polarizer cycles through 180° , the azimuth angle of the surface normal is ambiguous (ϕ or $\phi + 180^\circ$). The reflected light vector is coplanar with the reflection plane, defined as the plane spanned by the incident light and surface normal vectors. The reflection plane, which is oriented identically at the azimuth angle ϕ and at $\phi + 180^\circ$, is defined on a certain x - y plane angled between its own projection on the x - y plane and the x axis. Because the images were captured by a camera, we set the x and y axes as the image coordinates and the camera's z axis as the optical axis. Figure 3 illustrates the relationship between the surface normal and the azimuth angle ϕ obtained from polarization. Note that the surface normal cannot be uniquely determined because polarization obtains only the orientation of the reflection plane, which includes many surface normals.

3.2 Relation between polarization and normal

We projected unpolarized light onto the object and observed the diffusely reflected light passing through the polarizer. Figure 3 shows the situation in which the brightness was maximized (i.e., reached I_{\max}).

In the coordinate system shown in Fig. 3, we projected a surface normal onto the x - y plane, forming a vector on the x - y plane. The angle between

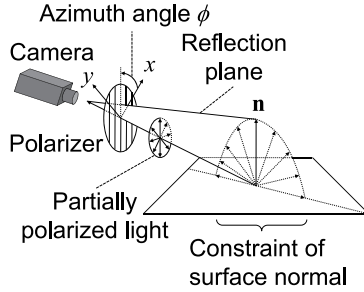


Fig. 3 Relationship between the surface normal and reflection plane observed from a single viewpoint

this vector and the x axis was denoted as the azimuth angle ϕ . The reflection plane was defined as the plane formed by the surface normal and the viewing direction. If the polarizer angle coincides with the plane of reflection, the brightness will be minimized (I_{\min}) for specular reflection and maximized (I_{\max}) for diffuse reflection. In this study, we assumed diffuse-dominant image pixels, meaning that all pixels were diffusely reflected. Therefore, the polarizer angle at which I_{\max} was observed coincided with ϕ .

We further assumed that the scene was illuminated by a single light source placed very close to the camera. This assumption is consistent with many real-world situations, as shape-from-shading is valid in small spaces. If sufficient space is available, the light source can be moved and photometric stereo is more precise than shape-from-shading. Therefore, shape-from-shading should be limited to narrow environments such as endoscopy environments, in which the light source cannot be moved and should be attached close to the camera.

When a single light is located close to the camera, diffuse reflection occurs over almost the entire surface. The exception is the point from which the surface normal points toward the camera. In both diffuse and specular reflection, the degree of polarization is zero when the surface normal coincides with the viewer (light) direction. At this point, the azimuth angle cannot be obtained because the light is perfectly unpolarized, but the surface normal is known to point toward the camera because the degree of polarization is zero.

To summarize, the azimuth angle of the surface normal can be determined from the polarization. However, because the polarizer cycle is 180° , the correct azimuthal angle is either ϕ or $\phi + 180^\circ$.

4 Shape detection from shading and polarization

4.1 Surface normal estimation

The shading information can be obtained as the observed brightness I divided by the albedo ρ . In this study, the directions of the light source and camera were almost identical and equal to $\mathbf{l} = (0, 0, 1)^\top$. Note that in this coordinate

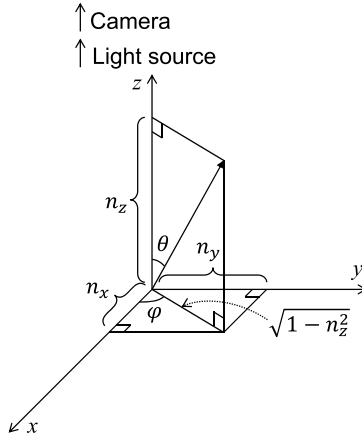


Fig. 4 Relationship between surface normal and azimuth angle in the present coordinate system

system, the camera direction coincides with the z axis. Therefore, the z value of the surface normal can be obtained as

$$n_z = \frac{I}{\rho}. \quad (3)$$

Rewriting Eq. (3), we get Eq. (4):

$$n_z = \cos \theta. \quad (4)$$

Figure 4 shows the relationship between the surface normal and the obtained azimuth angle. As the azimuth angle obtained from polarization has 180° ambiguity, the surface normal vector \mathbf{n} and ambiguous azimuth angle ϕ are related as

$$\frac{n_x}{\sqrt{1 - n_z^2}} = \begin{cases} \cos(\phi) \\ \cos(\phi + 180^\circ) \end{cases}, \quad (5)$$

$$\frac{n_y}{\sqrt{1 - n_z^2}} = \begin{cases} \sin(\phi) \\ \sin(\phi + 180^\circ) \end{cases}. \quad (6)$$

4.2 Disambiguation using the brightness gradient

Equations (5) and (6) give two possible candidates of the surface normal: ϕ or $\phi + 180^\circ$, one of which is the correct azimuth angle. The correct surface normal is decided from the brightness gradient of the pixels neighboring the target pixel. The target object is assumed to be piecewise convex. In the example of Fig. 5, the right pixel is brighter than the left pixel. As the light and camera directions are the same and the object is convex, the x component

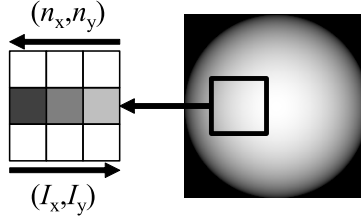


Fig. 5 Determining the orientation of the surface normal

of the surface normal is heading left. Applying the same procedure to the y axis, the judgment is mathematically described by Eq. (7), which denotes that the vector (n_x, n_y) opposes the vector (I_x, I_y) .

$$n_x I_x + n_y I_y < 0. \quad (7)$$

The pixel-brightness gradient is calculated as follows:

$$I_x = \frac{1}{2} (I(x+1, y) - I(x-1, y)), \quad (8)$$

$$I_y = \frac{1}{2} (I(x, y+1) - I(x, y-1)). \quad (9)$$

Where $I(x, y)$ is the brightness of the target pixel. Note that the following hold:

$$I_x = \frac{1}{2} (\rho \mathbf{n}(x+1, y) \cdot \mathbf{l} - \rho \mathbf{n}(x-1, y) \cdot \mathbf{l}), \quad (10)$$

$$I_y = \frac{1}{2} (\rho \mathbf{n}(x, y+1) \cdot \mathbf{l} - \rho \mathbf{n}(x, y-1) \cdot \mathbf{l}). \quad (11)$$

As the albedo ρ is constant and the light direction \mathbf{l} is fixed, the image gradient contains the information on the surface normal \mathbf{n} .

Using Eq. (7), we can determine whether Eq. (5) or Eq. (6) defines the correct ϕ . The correct ϕ is the direction of decreasing pixel brightness. Therefore, if $I_x \cos \phi + I_y \sin \phi < 0$, the surface normal components n_x and n_y can be calculated as

$$\begin{aligned} n_x &= \sqrt{1 - n_z^2} \cos(\phi), \\ n_y &= \sqrt{1 - n_z^2} \sin(\phi). \end{aligned} \quad (12)$$

Otherwise, if $I_x \cos \phi + I_y \sin \phi > 0$, the surface normal components n_x and n_y can be calculated from Eq. (13).

$$\begin{aligned} n_x &= \sqrt{1 - n_z^2} \cos(\phi + \pi), \\ n_y &= \sqrt{1 - n_z^2} \sin(\phi + \pi). \end{aligned} \quad (13)$$

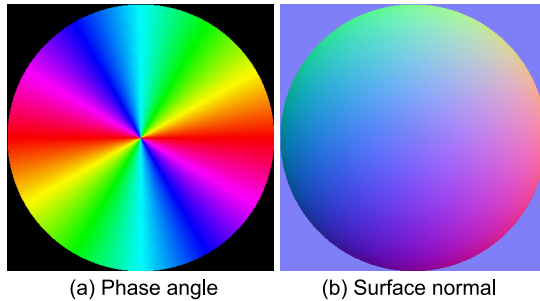


Fig. 6 Pseudo-color representations of (a) azimuth angle with 180° ambiguity and (b) a surface normal

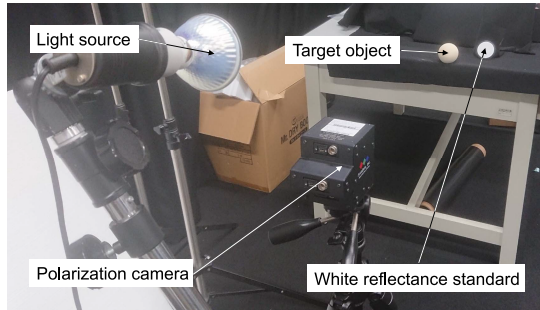


Fig. 7 Experimental environment.

5 Experiments

Panels (a) and (b) of Fig. 6 display the pseudo-color representations of an azimuth angle with 180° ambiguity and a surface normal, respectively. This section displays the experimental results in this pseudo-color representation.

5.1 Experimental setup

The proposed method was experimentally evaluated on real objects in a dark room (Fig. 7). The light source and camera were placed in almost the same location. The polarization camera is shown in Fig. 8, and its specifications are listed in Table 1. The polarization camera captures a single image with linear polarization parameters. We also captured a white-reflectance standard image with complete diffuse reflection (see Fig. 9). On this white plate, which completely depolarizes the light, we calibrated the polarization parameters of the camera.



Fig. 8 Polarization camera.

Table 1 Polarization camera specifications.

| | |
|-----------------|--|
| Manufacturer | FluxData Inc. |
| Product name | FD1665P |
| Sensor | Sony ICX414 x3 1/2CCD (charge-coupled device) color |
| Resolution | 659 × 494 |
| Pixel size | 9.9 μm × 9.9 μm |
| Configuration | Polarization 3 channel (0°, 45°, and 90°) |
| Frame rate | 74 fps |
| Interface | 1394/b |
| Software | Capture software & Development toolkit |
| Lens | Nikon 24mm f/2.8 |
| Internal camera | BASLER Inc., Scout OEM (original equipment manufacturer) on-board camera x3 |



Fig. 9 Image of the white-reflectance standard

5.2 Experiment on simulated data

This subsection presents the experimental results of the simulation data. The input image shown in Fig. 10 was computationally generated from the known geometry. An azimuth angle with 180° ambiguity is shown in Fig. 11. Applying the proposed method, the surface normals were calculated from the data shown in Figs. 10 and 11, and are shown in Fig. 12. These surface normals were

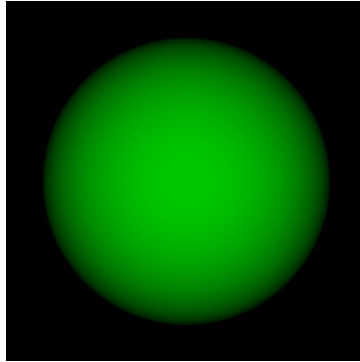


Fig. 10 Input data (brightness)

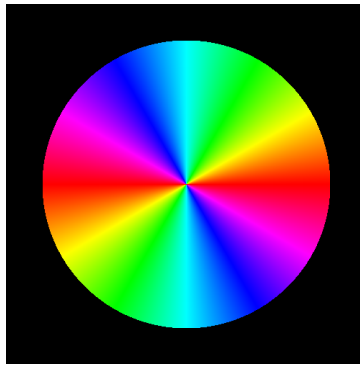


Fig. 11 Input data (azimuth angle with 180° ambiguity)

Table 2 Error between the obtained and true surface normals

| | |
|---------------------|-------|
| Average error [rad] | 0.000 |
| Minimum error [rad] | 0.000 |
| Maximum error [rad] | 0.000 |

integrated to obtain a three-dimensional (3D) geometrical shape (see Figs. 13 and 14 for front and side views, respectively). The errors between the obtained and true surface normals are listed in Table 2, and are mapped as color and gray images in Figs. 15 and 16, respectively.

5.3 Performance evaluation of our method and an existing method

Mahmoud et al. [19] also estimated the surface normal from polarization and shading. The surface normals estimated from Mahmoud et al. and our method are compared in panels (1a) and (1b) of Fig. 17, respectively. The input to

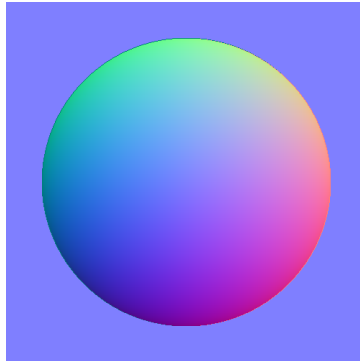


Fig. 12 Surface normals estimated by the proposed method

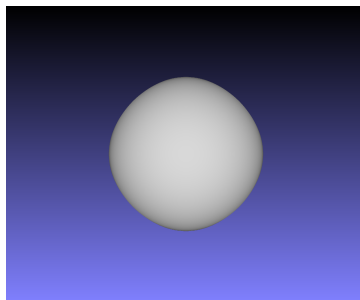


Fig. 13 Reconstructed shape (front view)

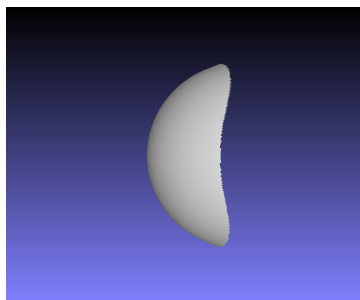


Fig. 14 Reconstructed shape (side view)

both models was a computer-generated image of a hemisphere with added noise.

Mahmoud et al.'s method is invalid when the camera and light directions coincide, whereas our method is invalid when the camera and light directions differ. The algorithms of the two methods are quite different, and have distinct

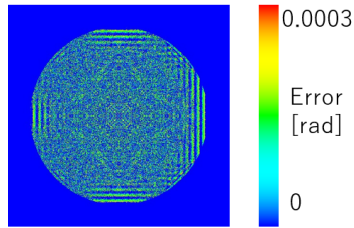


Fig. 15 Error map (color)

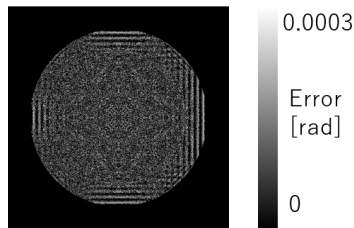


Fig. 16 Error map (gray)

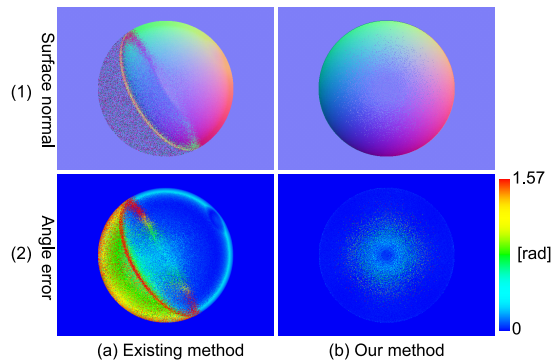


Fig. 17 Comparison results of our method and an existing method: (1) Surface normal, (2) angular error, (a) result of the existing method, and (b) result of the proposed method

advantages and disadvantages. Therefore, these two methods are complementary, and their utilities are mutually beneficial.

However, Mahmoud et al.'s method cannot estimate the shadowed area. On the other hand, our method does not cause shadow since the light source direction is almost the same as the viewing direction. As shown in Fig. 17 (a), the light was directed from the upper-right and the lower-left part of the object was shadowed.

As Mahmoud et al. used the degree of polarization, the surface normal in their method was erroneous at the center of the sphere where the polarization degree was low and noise-sensitive (Fig. 17 (a)). The surface normal in our

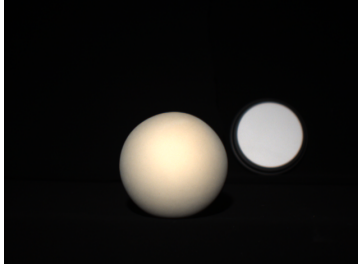


Fig. 18 Input data (brightness) of the real-data evaluation

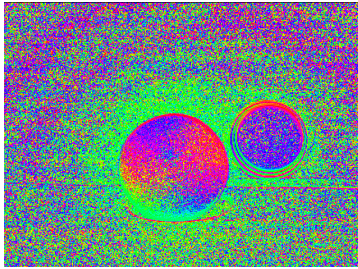


Fig. 19 Input data (azimuth angle with 180° ambiguity) of the real-data evaluation

method, which uses the phase angle, was also erroneous at the center of the sphere because the phase angle is sensitive to noise at low polarization degrees (Fig. 17 (b)). These disadvantages are inherent in any shape-from-polarization technique.

Mahmoud et al. disambiguated the azimuth angle problem using the shading information. In their approach, the ambiguity is difficult to solve when the phase-angle direction is orthogonal to the light direction.

5.4 Performance evaluation on real-data

The real-data evaluation was performed on a spherical object, on which the true surface normal is mathematically known. The input brightness and input azimuth angle with 180° ambiguity are shown in Figs. 18 and 19, respectively. Using these input data, the proposed method calculated the surface normals of the sphere (see Fig. 20). Integrating the surface normal, we obtained the 3D geometrical shapes shown in Figs. 21 (frontal view) and 22 (side view). The errors between the obtained and true surface normals are listed in Table 3 and are mapped as color and gray-scale images in Figs. 23 and 24, respectively.

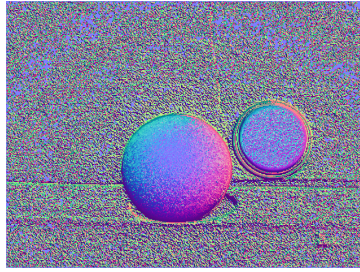


Fig. 20 Surface normals estimated by the proposed method on the input data of Figs. 18 and 19

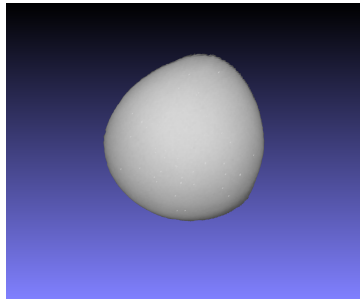


Fig. 21 Reconstructed 3D shape (front view) of the spherical object

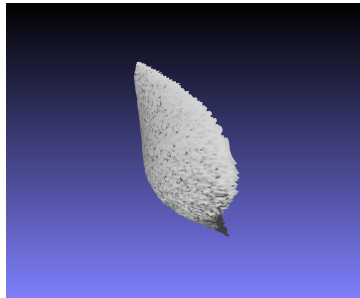


Fig. 22 Reconstructed 3D shape (side view) of the spherical object

Table 3 Errors between obtained and true surface normals

| | |
|---------------------|-------|
| Average error [rad] | 0.449 |
| Minimum error [rad] | 0.002 |
| Maximum error [rad] | 2.097 |

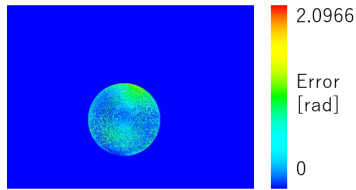


Fig. 23 Error map (color) of the spherical object

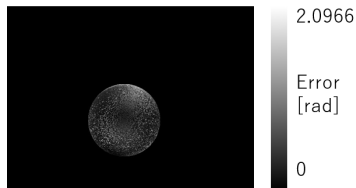


Fig. 24 Error map (gray) of the spherical object



Fig. 25 Pig-shaped target object in the real-data evaluation

5.5 Experiments on various real objects

This subsection evaluates the proposed method on real objects. A single set of input data was captured from a single viewpoint under a single light source. The input data were a brightness image and an azimuth angle image with 180° ambiguity. The brightness and angle data of the pig-like object shown in Fig. 25 are shown in Figs. 26 and 27, respectively, and the surface normals obtained by the proposed method are shown in Fig. 28. After integrating the surface normals, we obtained the 3D geometrical shapes shown in Figs. 29 (front view), 30 (side view), and 31 (close-up view).

Next, the proposed method was evaluated on the duck-shaped object shown in Fig. 32. The brightness and azimuth angle images of this object are shown in Figs. 33 and 34, respectively, and the obtained surface normals are shown



Fig. 26 Input image (brightness) in the pig-shaped real-data evaluation

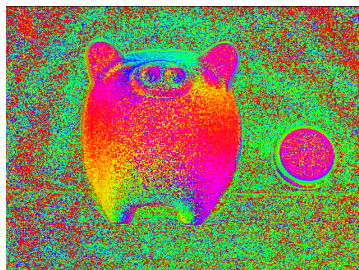


Fig. 27 Input image (azimuth angle with 180° ambiguity) in the pig-shaped real-data evaluation

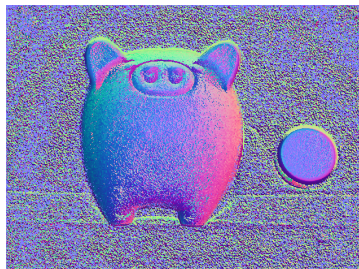


Fig. 28 Estimated surface normal in the pig-shaped real-data evaluation

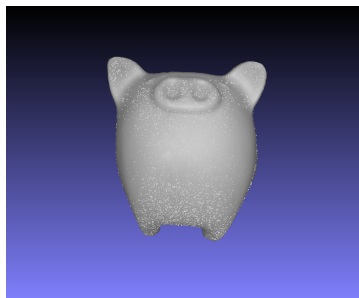


Fig. 29 Reconstructed 3D shape (front view) of the pig-shaped object

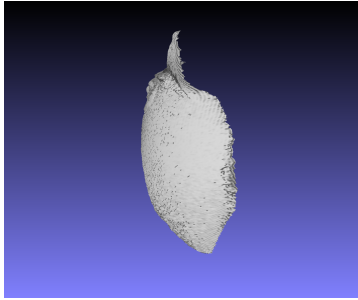


Fig. 30 Reconstructed 3D shape (side view) of the pig-shaped object

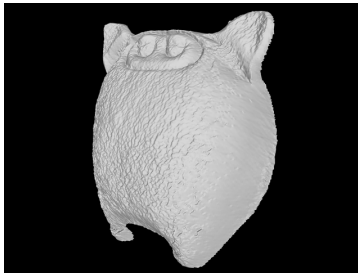


Fig. 31 Reconstructed 3D shape (close-up) of the pig-shaped object



Fig. 32 Duck-shaped target object

in Fig. 35. Integrating these surface normals, we obtained the 3D geometrical shapes shown in Figs. 36 (front view), 37 (side view), and 38 (close-up view).

The proposed method assumes a continuous target object. To assess the extent to which the proposed method was affected by depth gaps, we also evaluated the method on a non-continuous object (the rabbit-shaped object shown in Fig. 39). The captured brightness and azimuth angle images are presented in Figs. 40 and 41, respectively. The surface normals estimated using the proposed method are shown in Fig. 42. Integrating these surface normals, we retrieved the 3D geometrical shapes shown in Figs. 43 (front view), 44 (side view), and 45 (close-up view).



Fig. 33 Input image (brightness) of the duck-shaped object in the real-data evaluation

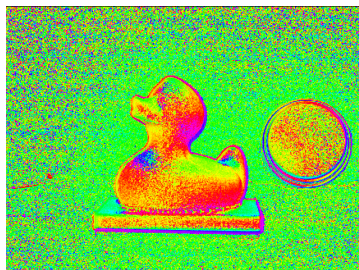


Fig. 34 Input image (azimuth angle with 180° ambiguity) of the duck-shaped object in the real-data evaluation

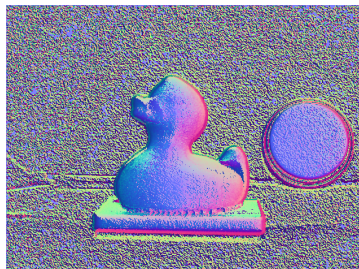


Fig. 35 Estimated surface normal of the duck-shaped object in the real-data evaluation

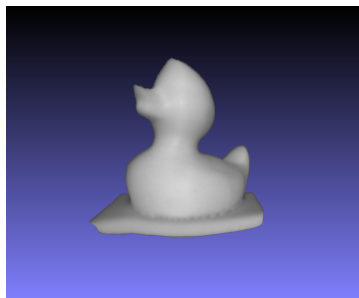


Fig. 36 Reconstructed 3D shape (front view) of the duck-shaped object

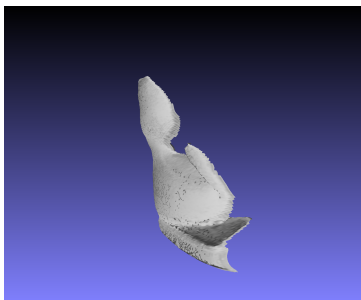


Fig. 37 Reconstructed 3D shape (side view) of the duck-shaped object

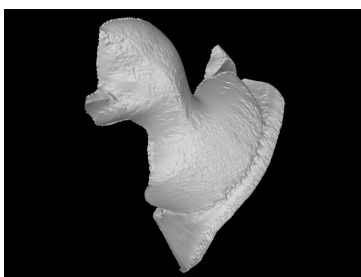


Fig. 38 Reconstructed 3D shape (close-up) of the duck-shaped object



Fig. 39 Rabbit-shaped target object



Fig. 40 Input image (brightness) of the rabbit-shaped object in the real-data evaluation

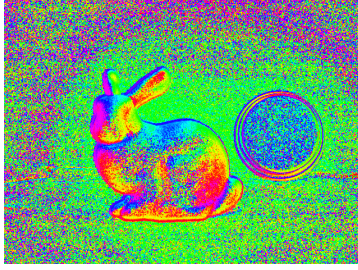


Fig. 41 Input image (azimuth angle with 180° ambiguity) of the rabbit-shaped object in the real-data evaluation

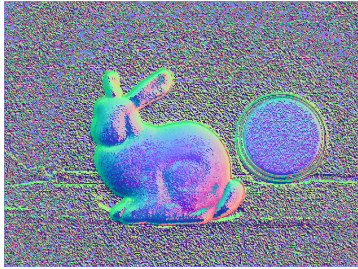


Fig. 42 Estimated surface normal of the rabbit-shaped object in the real-data evaluation



Fig. 43 Reconstructed 3D shape (front view) of the rabbit-shaped object

The proposed method assumes that the object is locally convex. To determine the extent to which the proposed method is affected by concavity, we performed an additional evaluation of the target object shown in Fig. 46. The input brightness and azimuth angle images are shown in Figs. 47 and 48, respectively, and the surface normals estimated using the proposed method are presented in Fig. 49. Integrating these surface normals, we obtained the 3D geometrical shapes shown in Figs. 50 (front view), 51 (side view), and 52 (close-up view).

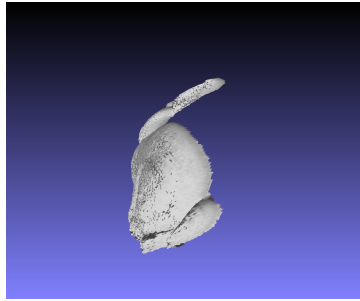


Fig. 44 Reconstructed 3D shape (side view) of the rabbit-shaped object

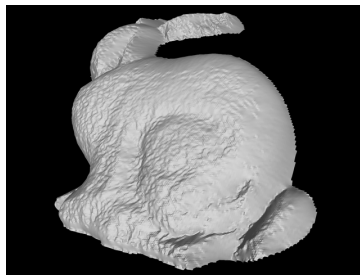


Fig. 45 Reconstructed 3D shape (close-up) of the rabbit-shaped object



Fig. 46 Dinosaur-shaped target object



Fig. 47 Input image (brightness) of the dinosaur-shaped object in the real-data evaluation

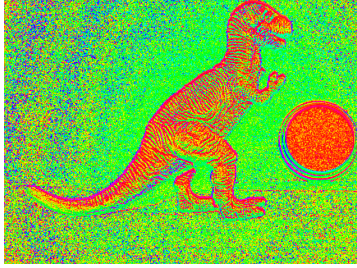


Fig. 48 Input image (azimuth angle 180° ambiguity) of the dinosaur-shaped object in the real-data evaluation

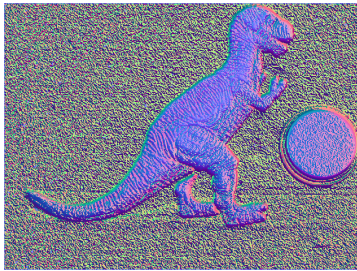


Fig. 49 Estimated surface normal of the dinosaur-shaped object in the real-data evaluation



Fig. 50 Reconstructed 3D shape (front view) of the dinosaur-shaped object

5.6 Discussion

As shown in the dinosaur results (Figs. 50 and 51), the non-smooth surface of the object was well reconstructed by the proposed method. Although the proposed method assumes a locally convex object, it is not restricted to globally convex objects. For example, the surface in Fig. 53 (a) is locally convex rather than globally convex. As the concave part is infinitesimally small, it is ignorable and will not affect the performance of the proposed method. In contrast, the surface in Fig. 53 (b) is dominated by concave parts and cannot be processed by the proposed method.

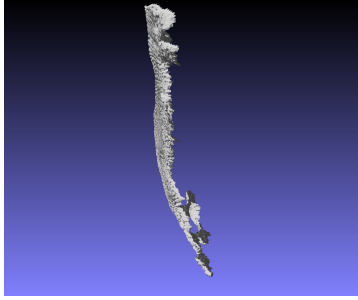


Fig. 51 Reconstructed 3D shape (side view) of the dinosaur-shaped object

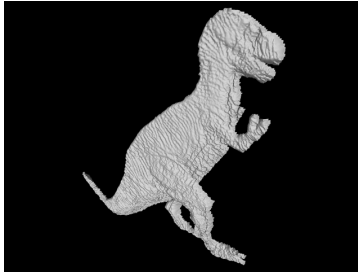


Fig. 52 Reconstructed 3D shape (close-up) of the dinosaur-shaped object

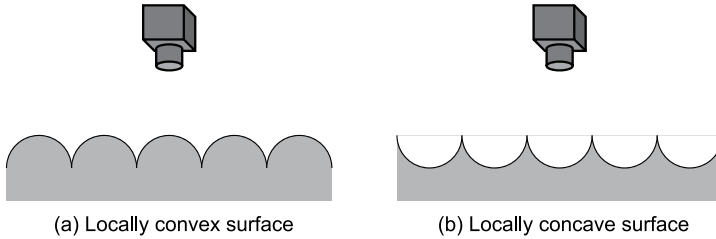


Fig. 53 Convexity and concavity of the object surface: (a) piecewise convex surface on which the proposed method can be applied, and (b) a piecewise concave surface on which the proposed method cannot be applied

The result of the dinosaur-shaped object (Fig. 52) was flatter than the actual shape. Note that local convexity is required for Eqs. (8) and (9). The image gradient was calculated along four neighboring pixels. Due to this finite-image resolution, our disambiguation fails at the boundaries of convex/concave parts. The error at the one-pixel-wide boundary can be ignored, but if the surface contains many concave parts, the error will accumulate to non-negligible levels. For the same reason, errors appeared on the concave part of the neck of the duck (Fig. 37) and rabbit (Fig. 44).

An interesting aspect of the proposed method is the non-requirement of a smoothness prior. Many methods add a smoothness constraint to alleviate the difficulty of the shape-from-shading problem. Unlike these methods, the proposed method does not need to smooth the surface. If a smooth result is required, the rough result of our method can be smoothed by simple image processing.

When processed by our method, the polarization data yield a noisy surface normal. Unlike specular reflection, diffuse reflection has a low degree of polarization, meaning that the input data are sensitive to noise. As the proposed method must use the polarization of diffuse reflection, the noise problem cannot be avoided in the current version, and requires a drastic change of our method. This change will be tackled in our future work.

6 Conclusion

We proposed a method that estimates a surface normal from the shading and polarization information. In a mathematical analysis, we indicated that the proposed method can reliably and robustly estimate surface normals. Next, we experimentally fortified our claim that the shading and polarization data can stably obtain the surface normals in single images. Unfortunately, the proposed method cannot be applied to multi-colored objects, but this disadvantage is common in shape-from-shading methods. Overcoming this problem will be a challenging task, and is earmarked for the near future.

7 Declarations

Conflict of interest

The authors declare that they have no competing interests.

References

1. T. Rindfleisch, "Photometric method for lunar topography," *Photogrammetric Engineering*, **32**(2), 262–277 (1966).
2. B. K. P. Horn, "Obtaining shape from shading information," in *The Psychology of Computer Vision*, P. H. Winston (Ed.), McGraw-Hill, New York, 115–155 (1975).
3. B. K. P. Horn and M. J. Brooks, "The variational approach to shape from shading," *Computer Vision, Graphics, and Image Processing*, **33**(2), 174–208 (1986). [doi:10.1016/0734-189X(86)90114-3].
4. B. K. P. Horn, "Height and gradient from shading," *International Journal of Computer Vision*, **5**, 37–75 (1990). [doi:10.1007/BF00056771].
5. R. Zhang, P. S. Tsai, J. E. Cryer, and M. Shah, "Shape-from-shading: a survey," *IEEE Transactions on Pattern Analysis and Machine Intelligence*, **21**(8), 690–706 (1999). [doi:10.1109/34.784284].
6. J.-D. Durou, M. Falcone, and M. Sagona, "Numerical methods for shape-from-shading: a new survey with benchmarks", *Computer Vision and Image Understanding*, **109**(1), 22–43 (2008). [doi:10.1016/j.cviu.2007.09.003].

7. R. J. Woodham, "Photometric method for determining surface orientation from multiple images," *Optical Engineering*, **19**(1), 139–144 (1980). [doi:10.1117/12.7972479].
8. L. B. Wolff and T. E. Boult, "Constraining object features using a polarization reflectance model," *IEEE Transactions on Pattern Analysis and Machine Intelligence*, **13**(7), 635–657 (1991). [doi:10.1109/34.85655].
9. S. Rahmann and N. Canterakis, "Reconstruction of specular surfaces using polarization imaging," in *Proceedings of IEEE Computer Society Conference on Computer Vision and Pattern Recognition*, 149–155 (2001). [doi:10.1109/CVPR.2001.990468].
10. S. Rahmann, "Reconstruction of quadrics from two polarization views," in *Proceedings of Iberian Conference on Pattern Recognition and Image Analysis*, 810–820 (2003). [doi:10.1007/978-3-540-44871-6_94].
11. G. A. Atkinson and E. R. Hancock, "Shape estimation using polarization and shading from two views," *IEEE Transactions on Pattern Analysis and Machine Intelligence*, **29**(11), 2001–2017 (2007). [doi:10.1109/TPAMI.2007.1099].
12. G. A. Atkinson and E. R. Hancock, "Recovery of surface orientation from diffuse polarization," *IEEE Transactions on Image Processing*, **15**(6), 1653–1664 (2006). [doi:10.1109/TIP.2006.871114].
13. C. P. Huynh, A. Robles-Kelly, and E. R. Hancock, "Shape and refractive index from single-view spectro-polarimetric images," *International Journal of Computer Vision*, **101**, 64–94 (2013). [doi:10.1007/s11263-012-0546-3].
14. O. Drbohlav and R. Šára, "Specularities reduce ambiguity of uncalibrated photometric stereo," in *A. Heyden, G. Sparr, M. Nielsen, P. Johansen (eds) Computer Vision – ECCV 2002*, Springer, Berlin, Heidelberg, **2351**, 46–62 (2002). [doi:10.1007/3-540-47967-8_4].
15. T. T. Ngo, H. Nagahara, and R. Taniguchi, "Shape and light directions from shading and polarization," in *IEEE Conference on Computer Vision and Pattern Recognition*, 2310–2318, 2015. [doi:10.1109/CVPR.2015.7298844].
16. S. Tozza, W. A. P. Smith, D. Zhu, R. Ramamoorthi, and E. R. Hancock, "Linear differential constraints for photo-polarimetric height estimation," in *IEEE International Conference on Computer Vision*, 2298–2306 (2017). [doi:10.1109/ICCV.2017.250].
17. F. Logothetis, R. Mecca, F. Sgallari, and R. Cipolla, "A differential approach to shape from polarisation: a level-set characterisation," *International Journal of Computer Vision*, **127**, 1680–1693 (2019). [doi:10.1007/s11263-018-1127-x].
18. D. Miyazaki and S. Hashimoto, "Uncalibrated photometric stereo refined by polarization angle," *Optical Review*, **28**, 119–133 (2021). [doi:10.1007/s10043-021-00640-0].
19. A. H. Mahmoud, M. T. El-Melegy, and A. A. Farag, "Direct method for shape recovery from polarization and shading," in *IEEE International Conference on Image Processing*, 1769–1772 (2012). [doi:10.1109/ICIP.2012.6467223].
20. W. A. P. Smith, R. Ramamoorthi, and S. Tozza, "Height-from-polarisation with unknown lighting or albedo," *IEEE Transactions on Pattern Analysis and Machine Intelligence*, **41**(12), 2875–2888 (2019). [doi:10.1109/TPAMI.2018.2868065].